2017

Spin flip loss in magnetic confinement of ultracold neutrons for neutron lifetime experiments

A. Steyerl

K. K. H. Leung

See next page for additional authors

Citation/Publisher Attribution

Albert Steyerl, K. K. H. Leung, Charles Kaufman, Gerhard Müller, and Surendra S. Malik *Spin flip loss in magnetic confinement of ultracold neutrons for neutron lifetime experiments.* Phys. Rev. C **95** (2017) 035502, pp. 1-1.
Available at: http://dx.doi.org/PhysRevC.95.035502

Spin flip loss in magnetic confinement of ultracold neutrons for neutron lifetime experiments

A. Steyerl,[1,*] K. K. H. Leung,[2,†] C. Kaufman,[1,‡] G. Müller,[1,§] and S. S. Malik[1,‖]
[1]*University of Rhode Island, Kingston, Rhode Island 02881, USA*
[2]*North Carolina State University, Raleigh, North Carolina 27695, USA*
(Received 14 November 2016; published 22 March 2017)

We analyze the spin flip loss for ultracold neutrons in magnetic bottles of the type used in experiments aiming at a precise measurement of the neutron lifetime, extending the one-dimensional field model used previously by Steyerl *et al.* [Phys. Rev. C **86**, 065501 (2012)] to two dimensions for cylindrical multipole fields. We also develop a general analysis applicable to three dimensions. Here we apply it to multipole fields and to the bowl-type field configuration used for the Los Alamos UCNτ experiment. In all cases considered the spin flip loss calculated exceeds the Majorana estimate by many orders of magnitude but can be suppressed sufficiently by applying a holding field of appropriate magnitude to allow high-precision neutron lifetime measurements, provided other possible sources of systematic error are under control.

DOI: 10.1103/PhysRevC.95.035502

I. INTRODUCTION

The neutron lifetime τ_n is an important parameter in nuclear physics, particle physics, and cosmology. τ_n can be combined with the neutron β-decay ($n \to p + e^- + \bar{\nu}_e$) correlation coefficients to determine the universal weak interaction vector and axial-vector coupling constants whose values allow searches for semileptonic scalar and tensor currents beyond the standard model [1–4]. A τ_n of reliable precision is also needed for calculations of the neutrino flux expected from solar and reactor sources, including detection efficiencies [5–7], as well as in big bang nucleosynthesis calculations. At present, we are confronted by an apparent discrepancy of about three standard deviations between the average τ_n from ultracold neutron (UCN) storage experiments and the τ_n from cold neutron beam experiments as outlined in the next paragraph. It is the leading source of uncertainty in predictions of the primordial abundance of ^{4}He [8–10].

Experiments determining τ_n employ either a beam of cold neutrons or an ensemble of trapped ultracold neutrons (UCN) (see [11–16] for reviews of τ_n experiments). In-beam experiments count reaction products (p or e^-) emerging from an exactly specified section of the beam while the trapping method involves loading UCNs into a "neutron bottle" and counting the "survivors" as a function of the holding time. The most common τ_n experiments to date have used material traps where the neutrons reflect off the neutron-optical potential of the wall. This requires correction of measured storage lifetimes for reflection losses. Measuring procedures have been applied which take into account, as well as possible, even loss channels which are not well understood, such as surface contamination by hydrogenous substances.

Wall losses can be avoided by confining the UCNs in "magnetic neutron bottles," utilizing the interaction energy $-\boldsymbol{\mu} \cdot \mathbf{B}$ between the neutron magnetic moment $\mu = -60.3$ neV/T with a static nonuniform magnetic field $\mathbf{B}$ to establish a closed trapping region. In this scheme, only the neutrons in one spin state can be stored; those in the other spin state are attracted towards the wall and lost. In the field configurations commonly applied the field increases toward the wall, thus neutrons in the low-field seeking state with spin parallel to $\mathbf{B}$ (i.e., $\boldsymbol{\mu}$ antiparallel to $\mathbf{B}$) are stored and should, ideally, experience no losses other than β decay, provided that depolarization, i.e., the spin flip to the opposite spin state, is sufficiently suppressed.

Until recently, UCN depolarization estimates [17,18] have been based on Majorana's quasiclassical result [19] for a model where a particle with magnetic moment moves with constant velocity vector through an infinitely extended nonuniform magnetic field of specific form. For field parameters as currently used for magnetic UCN storage the probability D of a spin flip away from the field direction would be of order $D \sim e^{-10^6}$, thus immeasurably small.

Walstrom *et al.* [20], in 2009, pointed out that the values of D for confined, rather than freely moving, neutrons are much larger. For a particular vertical path in the field of the Los Alamos gravito-magnetic UCN trap they calculated $D \sim 10^{-20}$–10^{-23}, which is much larger than the Majorana estimate but still negligible in any actual or projected neutron lifetime experiment.

In Refs. [21,22] we extended this theory to general orbits with both vertical and horizontal velocity components, using the model of an ideal Halbach magnetic field $\mathbf{B}$ where the magnitude B only depends on the vertical position. We found that the lateral motion in the plane where the Halbach field rotates is of critical importance. Taking it into account increases the spin flip loss thus calculated by some 10 orders of magnitude to $D \sim 10^{-12}$ for a field minimum (holding field) of $B_h \approx 5$ mT. This translates into a spin flip loss rate that is a fraction $\sim 10^{-4}$ of the β-decay rate and decreasing rapidly with larger holding field.

The analysis in Refs. [20,21] is based on the following concepts: For the one-dimensional (1D) field model of [21], the potential $V(z) = gz - \mu B(z)/m = gz + |\mu| B(z)/m$ for the high-field repelled $|+\rangle$ spin state of a neutron with mass

*asteyerl@uri.edu
†kkleung@ncsu.edu
‡chuck@uri.edu
§gmuller@uri.edu
‖smalik@uri.edu

m depends only on the vertical z coordinate. In this model the neutrons are exposed to a uniform gravitational field $-g\hat{\mathbf{z}}$ and a nonuniform magnetic field of magnitude $B(z)$. They perform an oscillatory motion with turning points (TP) at the lower and upper horizontal equipotential surfaces (ES) where $v_z = 0$ and the potential is $V = (E/m) - v_\perp^2/2$. Here E is the neutron energy; v_z and $v_\perp = \sqrt{v_x^2 + v_y^2}$ are the vertical and horizontal velocity components, respectively. $v_\perp$ is constant for the 1D field model.

As the particle moves from one TP to the next, starting out in a pure $|+\rangle$ spin state, its wave component for the $|-\rangle$ spin state increases. It may change over many orders of magnitude [20,21], peaking at critical points where the field magnitude B is small and the vector $\mathbf{B}$ rotates rapidly in the reference frame of the moving particle. The spin flip probability is "measured" only at the next TP where, in the Copenhagen interpretation, the wave function collapses and UCNs in the $|+\rangle$ state return to the trapping region while the $|-\rangle$ projection separates in space and quickly becomes lost. Conceptually, the "measurement" could be made by an ideal neutron detector placed just next to the TP, which would intersect the UCNs in the "wrong" spin state as they exit the storage space. This "measurement" resets the UCN wave function to a pure initial $|+\rangle$ state for the next lap where the sequence of wave evolution and collapse at the following TP is repeated.

II. OUTLINE

In the present article we extend this approach to the analysis of depolarization in cylindrical multipole fields such as those described in Refs. [23–28], where the trapping fields are generated by Halbach arrays of permanent magnets [24–27] or, for [23,28] and, earlier [29], by superconducting currents. For these cylindrical configurations we use a 2D field model which enables us to obtain a semianalytic expression for the ensemble-averaged spin flip loss and which can be analyzed with no need to involve simulations. The results are consistent with the only experimental spin flip probabilities with varying holding field available so far [26].

For the cylindrical $2N$ pole we approximate the field in cylindrical coordinates r, ϕ, ζ as follows:

$$\begin{aligned} B_r &= B_{\max}(r/R)^{N-1}\sin(N\phi), \\ B_\phi &= B_{\max}(r/R)^{N-1}\cos(N\phi), \\ |\mathbf{B}| &= B(r) = \sqrt{B_\zeta^2 + B_{\max}^2(r/R)^{2N-2}}, \end{aligned} \tag{1}$$

where $N \geqslant 2$. ζ points along the cylinder axis and the holding field B_ζ is considered constant. $B_{\max}$ is the trapping field magnitude at the wall and the radius R (typically $\sim$5 cm) is much smaller than the length, which is of order 1 m. This justifies the neglect of gravity for horizontal configurations of this type [23] since the gravitational energy varies little over the trap radius. To assess the merits of model (1) in general we have performed 3D simulations including gravity both for the vertical and the horizontal cylindrical multipole configurations.

As a second application we extend the previous analysis [21] of depolarization for a 1D field model of the Los Alamos UCNτ trap [20,30,31] to the actual field in this magneto-gravitational trap with its asymmetrically double-curved wall in the shape of a bowl. As in Ref. [20] we approximate the field for the curved arrays of permanent magnets by that of the corresponding infinite planar array tangent to the bowl surface at the closest point on the bowl surface. We also use the same expressions for the flat-wall field, dubbed "smooth" [Eq. (5) of [20]], "one-way ripple" [Eq. (7)] and "two-way ripple" [Eq. (8)]. The "one-way ripple" takes into account the finite magnet size and the "two-way ripple" also includes the effect of iron shims between the magnets, a design feature not implemented for the current UCNτ system (status of 2016).

The theoretical approach is outlined in Sec. III, where we derive a first-order approximation to the spin flip probability from the spin-dependent Schrödinger-Pauli equation (SE), and in Sec. IV where we average these results over the ensemble of orbits in the field configurations of UCNτ and of multipole bottles. In Sec. V we derive a higher-order solution of the spin-dependent SE and show that it deviates very little from the first-order approximation. These various approaches are semiclassical since the field $\mathbf{B}(t)$ acting on the neutron spin is determined by the classical motion of the particle through the field. However, the results have been shown [20,21] to be consistent also with a fully quantum mechanical analysis starting from the spin and space dependent SE. We show in the Appendix that this equivalence also holds for our extension to arbitrary field configurations.

As in Refs. [20,21], we use the Wentzel-Kramers-Brillouin (WKB) approximation [32] to solve the SE. This is justified since the spatial variation of field variables is much slower than the variation of the UCN wave function. The scales are of order cm for gravity and $\mathbf{B}$, and of order μm or less for the wavelength. Thus the wave function for spin state $|+\rangle$ can be expressed in the WKB form except at a TP $z' = 0$, where its amplitude $1/\sqrt{k'_+(z')}$ diverges since the wave number k'_+ vanishes. [See Eq. (A12) for details.] Furthermore, due to the slow variation of field variables their gradients are small quantities.

III. SEMICLASSICAL APPROACH

Neutron lifetime experiments based on magnetic storage require that the spin follows the changes of field direction along the neutron path for a time much longer than the neutron lifetime, implying that the probability $|\alpha(t)|^2$ for spin $|+\rangle$, parallel to the local field, is always much larger than the small spin-flipped part $|\beta(t)|^2$. Therefore, in order to separate large terms in the SE [e.g. those in Eq. (6) below] from the small ones [those in Eq. (7)] it is advantageous to use a reference system which rotates with the field experienced by the moving particle. Thus we use the SE for spin 1/2 with quantization axis in the local field direction, as in Refs. [20,21]:

$$\begin{aligned} i\hbar\frac{d}{dt}&[\alpha(t)\chi^+(t) + \beta(t)\chi^-(t)] \\ &= |\mu|B[\alpha(t)\chi^+(t) - \beta(t)\chi^-(t)], \end{aligned} \tag{2}$$

where the spinors

$$\chi^+ = \begin{pmatrix} c \\ e_+ s \end{pmatrix} \quad \text{and} \quad \chi^- = \begin{pmatrix} e_- s \\ -c \end{pmatrix} \tag{3}$$

are the orthonormal basis vectors corresponding to the spin aligned in the direction of the local magnetic field $\mathbf{B}$ and opposite to it, respectively. Here $c = \cos(\theta/2)$, $s = \sin(\theta/2)$ and $e_\pm = e^{\pm i\phi}$ are given by the angles θ (polar) and ϕ (azimuthal) defining the direction of $\mathbf{B}(x,y,z)$ at the point $x(t),y(t),z(t)$ through which the particle passes along its trajectory at time t. For example, for the Los Alamos "bowl" we choose, as in Ref. [20], the fixed Cartesian coordinate system x,y,z, where z points vertically up. y (horizontal) and z define the vertical symmetry plane. In this plane ($x = 0$) the holding field points in the x-direction and we refer θ and ϕ to this fixed direction: $\theta = \arccos(B_x/B)$ and $\phi = \arctan(B_z/B_y)$. Similarly, for the cylindrical multipole field we refer θ and ϕ to the direction of the symmetry axis.

In the reference system moving with the particle, θ and ϕ depend on t. In Eq. (2) we need the temporal derivatives $\dot\chi^+(t)$ and $\dot\chi^-(t)$ [21]

$$\dot\chi^+ = A_{pp}\chi^+ + A_{pm}\chi^-, \quad \dot\chi^- = A_{mp}\chi^+ + A_{mm}\chi^-, \tag{4}$$

with time dependent coefficients

$$\begin{aligned} A_{pp} &= \frac{i}{2}\dot\phi(1-\cos\theta), \quad A_{pm} = -\frac{1}{2}e_+(\dot\theta + i\dot\phi\sin\theta), \\ A_{mp} &= -A^*_{pm}, \quad A_{mm} = A^*_{pp} = -A_{pp}. \end{aligned} \tag{5}$$

A_{mp} and A_{pp} are determined by the time derivatives of the field ($\dot\theta$ and $\dot\phi$). These are small quantities as compared to the wave frequency which is given by the Larmor frequency $\omega_L = 2|\mu|B/\hbar$. In practical cases, $|A_{pp}|$ and $|A_{mp}|$ are $\sim 10^{-4}\omega_L$ or less even at the field minima. Therefore, we will treat these quantities as small perturbations.

Using Eqs. (3)–(5) in Eq. (2) we obtain for the terms with χ^+ in first order

$$\dot\alpha + \frac{i\omega_L}{2}\alpha = 0, \tag{6}$$

and for those with χ^-

$$\dot\beta - \frac{i\omega_L}{2}\beta = -\alpha A_{pm} = \frac{\alpha}{2}e_+(\dot\theta + i\dot\phi\sin\theta). \tag{7}$$

In WKB approximation, the solutions of ordinary differential equations (ODEs) (6) and (7) are [20,21]

$$\alpha(t) = e^{-i\Theta/2}, \tag{8}$$

$$\beta(t) = -\frac{iA_{pm}}{\omega_L}e^{-i\Theta/2} = \frac{i}{2\omega_L}e_+(\dot\theta + i\dot\phi\sin\theta)e^{-i\Theta/2}, \tag{9}$$

where $\Theta = \int_0^t \omega_L(t')\,dt'$ is twice the phase angle accumulated since the previous TP. Since α and β have the same phase factor $e^{-i\Theta/2}$, the wave components α and β propagate between TPs as a unit (they do not run apart). This important feature had also been noted in Ref. [21].

From (9), the probability of finding the neutron in the spin-flipped state along the way to the next TP is

$$p(t) = |\beta(t)|^2 = \frac{\dot\theta^2(t) + \dot\phi^2(t)\sin^2\theta(t)}{4\omega_L^2(t)} = \frac{\Omega^2(t)}{4\omega_L^2(t)}. \tag{10}$$

$\Omega(t)$ is the frequency of field rotation about an axis normal to the plane defined by $\mathbf{B}$ and $\dot{\mathbf{B}}$ and can be expressed as $\Omega = |\mathbf{B}\times\dot{\mathbf{B}}|/B^2$. This form holds since $(\dot\theta^2 + \dot\phi^2\sin^2\theta)\,dt^2$ is the squared projection of vector $\dot{\mathbf{B}}\,dt$, as drawn from the tip of vector $\mathbf{B}$, onto the unit sphere. For any trajectory we determine the arrival time and the position of the TPs from the condition that the velocity component along the gradient of potential V vanishes, $\mathbf{v}\cdot\nabla V = 0$, since, at a TP, the particle momentarily moves along the ES at a stationary speed.

Equations (9) and (10) make use of an approximation which we will discuss in Sec. V in connection with the higher-order solution given in Eqs. (25) and (27). In short, this analysis shows the following features of $p(t)$: Starting from zero at a TP, $p(t)$ increases to the value given in Eq. (10) within a short time of order μs. Equation (10) holds over the entire remainder, typically 0.01–0.1 s, of the motion to the next TP where $p(t)$ is "measured." Equation (10) shows that the result depends only on the local field variables $\Omega(t)$ and $\omega_L(t)$. It does not depend on the path history; from (9), only the phase $-\Theta/2$ of $\beta(t)$ does. [This is similar to the behavior of $\alpha(t)$ shown in Eq. (8).]

For the sequence of TPs encountered along a neutron path of total duration $T_{\rm tot}$ we determine the spin flip rate between consecutive TPs at t_{i-1} and t_i by dividing $p(t_i)$, from (10), by the time interval $\Delta T_i = t_i - t_{i-1}$. Taking into account the probability $\Delta T_i/T_{\rm tot}$ of finding the particle on this path element the spin flip rate for the entire path becomes

$$1/\tau_{\rm dep} = \frac{1}{T_{\rm tot}}\sum_{i=1}^{n} p(t_i), \tag{11}$$

where n is the number of TPs encountered. Finally, the depolarization rate measured in the experiments is the ensemble average over all paths, which is determined by the source characteristics and by spectral cleaning. We assume an isotropic Maxwell spectrum, thus an energy independent phase space density (PSD). The Boltzmann factor e^{-E/k_BT} is close to unity since UCN energies E, which are of order $\lesssim 10^{-7}$ eV, are much lower than k_BT even for a low trap temperature T. The corresponding velocity dependence of the spectrum is $f(v) \sim v^2$ [for v up to the local trapping limit; from energy conservation, this limit depends on the local potential $V(x,y,z)$].

Relation (10) is also obtained in a fully quantum mechanical approach using the space and spin dependent SE in WKB approximation [20,21]. This equivalence holds for any field geometry, as shown in the Appendix.

IV. ENSEMBLE AVERAGE OF SPIN FLIP LOSS

In actual magnetic UCN storage systems it is difficult to make sure that the spectrum is isotropic and fills phase space uniformly up to the trapping limit. In practice this would require the complete removal of UCNs with energies slightly exceeding the limit. These tend to be in quasistable orbits lasting for times of the order of τ_n, thus affecting

the precision of a measurement of τ_n. Deviations from the Maxwell spectrum may also be due to the characteristics of the UCN source and of UCN transport to the trap but we will disregard these differences since they are expected to be of minor importance for the specific loss due to spin flip.

A. 1D field model

For the 1D field model of Ref. [21] the condition of constant PSD was taken into account as follows: The spin flip probability was averaged over the vertical velocity component v_{z0} in the plane $z = z_0$ where the gravitational downward force, $-mg$, is balanced by the magnetic upward force, $-\mu d|\mathbf{B}|/dz$. z_0 is the 1D equivalent of an elliptic fixed point O and $z = z_0$ is the only plane where UCNs of any energy E can reside, down to $E = 0$ and up to the maximum value for trapping. (Here and henceforth we set the potential $V = 0$ at O and assume that there are no other potential minima in the trapping region; this is the case for the field configurations presently used or proposed.) For any other height, the lower energy limit is nonzero. Therefore, to include all possible orbits in the averaging process we have to choose z_0 as the reference height, and since the statistical distribution of v_{z0} values is uniform for uniform PSD, the mean depolarization rate is given as the average of $1/\tau_{\rm dep}$ as a function of v_{z0}.

To analyze the depolarization between consecutive TPs we start trajectories from a TP, not from the fixed point O; so we have to connect the statistics at z_0, which is given by a uniform distribution of v_{z0}, with the distribution $P(z)$ of launching height z for given v_{z0}. $P(z)$ follows from energy conservation: The potential at the launching point is $V(z) = v_{z0}^2/2$, thus $(dV/dz)dz = v_{z0}dv_{z0}$. Therefore, to represent constant spacing in velocity space ($\Delta v_{z0} = $ const.) for orbits launched at height z we have to choose the density $P(z)$ of launching points proportional to

$$\frac{1}{\Delta z} = \frac{|dV(z)/dz|}{v_{z0}\,\Delta v_{z0}} = \frac{|dV(z)/dz|}{(\Delta v_{z0}\sqrt{2})\sqrt{V}},$$

thus

$$P(z) = \frac{|dV(z)/dz|}{\sqrt{V(z)}}, \tag{12}$$

where we have omitted the irrelevant constant factor $1/(\Delta v_{z0}\sqrt{2})$. In this form, $P(z)$ is neither normalized nor made dimensionless. This is not necessary since in the simulations described below we use von Neumann's acceptance or rejection method to implement probability distributions. For this purpose we only need the relative value $P/P_{\rm max}$, where $P_{\rm max}$ is the maximum value of P for the ensemble of trajectories.

B. General 3D field models

Now we adapt this result to arbitrary 3D field models as are relevant for the Los Alamos bowl [20]. In this system the asymmetry introduced by the choice of two different radii of curvature along the rows of Halbach field magnets helps to randomize the orbits, although fully mixing phase flow cannot be achieved. To select a representative sample of orbits for depolarization calculations we assume that most particles with energy E below the trapping limit will, at some time, be found at rest. (This would be the case for full phase mixing and is a reasonable approximation for UCNτ. Moreover, for the argument made below it suffices to assume that, at some time during storage, the particle is slowed down, by field gradients, to a small velocity, not necessarily to a full stop.) At the time of a momentary halt the particle has just reached the ES $V = E/m =$ constant. It will then be accelerated back into the region of lower potential in the direction perpendicular to the ES.

Taking these points as the initial position for simulated trajectories starting from rest, we make sure that the particle remains within the volume bounded by the ES with potential $V = E/m$ (as long as no spin flip to the $|-\rangle$ state takes place). The statistical distribution of launch points in space is determined by the following extension of (12) to 3D geometry: We relate the launching point to the fixed point O in the same way as for the 1D field model. Equating the initial energy $E = mV(x,y,z)$ with the kinetic energy at O, $E = mv_0^2/2$, we differentiate $V(x,y,z) = v_0^2/2$. This gives $\nabla V \cdot d\mathbf{s} = |\nabla V|\,ds = v_0\,dv_0$ where we have taken into account that the path element $d\mathbf{s}$ is parallel to the gradient of $V(x,y,z)$ at the launching point. Furthermore, in the immediate vicinity of O the potential is constant, thus the spatial density is stationary. Hence, to satisfy uniformity of PSD the density in velocity space must be uniform, $\Delta v_0 =$ constant, and we have to choose the spatial density of launching points proportional to

$$\frac{1}{\Delta s} = \frac{|\nabla V|}{v_0\,\Delta v_0} = \frac{|\nabla V|}{(\Delta v_0\sqrt{2})\sqrt{V}}.$$

As in Eq. (12) we can ignore the constant factor $1/(\Delta v_0\sqrt{2})$ and define

$$P(x,y,z) = \frac{|\nabla V(x,y,z)|}{\sqrt{V(x,y,z)}} \tag{13}$$

as the (non-normalized) probability distribution representing the number of launch points per unit volume at position (x,y,z).

We use this method to select random launching points for simulated orbits in UCNτ for the three field models—"smooth," "one-way ripple," and "two-way ripple"—and the toroidal-shaped holding field coil geometry described in Ref. [20]. We approximate the latter by a complete (360°), tightly wound torus, thus neglecting end effects and ripples for the holding field. Averaging the spin flip rate (11) over a sample of some 10^3 orbits, each of duration $T_{\rm tot} = 10$ s with $n \approx 100$ TPs, for four values of holding field B_{x0} at the bowl bottom, we obtain the depolarization rate $\langle 1/\tau_{\rm dep}\rangle$ shown in Table I. The results are consistent, within a factor

TABLE I. Mean depolarization rate $\langle 1/\tau_{\rm dep}\rangle$ (10^{-9}/s) for the Los Alamos UCNτ field.

B_{x0} (T)	Smooth	One-way ripple	Two-way ripple
0.1	0.022(1)	0.023(1)	0.024(1)
0.03	0.32(1)	0.33(1)	0.31(1)
0.01	1.6(1)	1.7(1)	1.9(1)
0.001	9.4(1)		

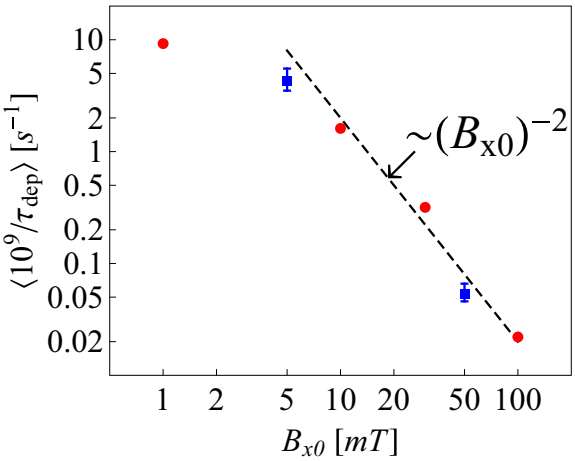

FIG. 1. Comparison of spin flip loss rate calculated in Ref. [21] for the Los Alamos UCNτ trap [20] using a 1D field model (blue squares) with the present 3D calculation for the smooth field given in Eq. (5) of [20] (red circles). In the range $B_{x0} \gtrsim 5$ mT the data are represented reasonably well by the power law $\langle 1/\tau_{dep}\rangle \sim B_{x0}^{-2}$, as shown by the dashed line.

of 2, with those given in Fig. 3 of Ref. [21] for the 1D field model: $\langle 1/\tau_{dep}\rangle \approx 4 \times 10^{-9}$ s^{-1} for $B_{x0} = 5$ mT and $\langle 1/\tau_{dep}\rangle \approx 5 \times 10^{-11}$ s^{-1} for $B_{x0} = 50$ mT. Figure 1 shows as squares the 1D calculation of [21] and as circles the present 3D calculations for the smooth-field model. In the range $B_{x0} \gtrsim 5$ mT the data are represented reasonably well by the proportionality $\langle 1/\tau_{dep}\rangle \sim B_{x0}^{-2}$ as indicated by the dashed line.

Table I shows that the field ripple has a minor effect on the net depolarization loss. This is plausible since the ripple only affects the immediate vicinity, of order mm, of the wall which contributes little to the spin flip since the adiabatic condition $\Omega \ll \omega_L$ is well satisfied in the region of high field strength near the wall.

C. Cylindrical multipole fields

1. *Results for the field model of Eq. (1)*

We use the field of an ideal cylindrical multipole given in Eq. (1), which does not take into account the deviations induced in the actual designs by the discrete geometry of electric currents [23,28], or by the permanent magnet blocks with constant magnetization within each block in the schemes of Refs. [20,24–27].

Equation (1) neglects gravity and assumes a uniform holding field B_ζ in the axial direction. With these simplifications, the field is determined only by the polar coordinates r and ϕ in the plane perpendicular to the axis. Moreover, the field magnitude B and the force $-|\mu|\,dB/dr$ acting on a $|+\rangle$ spin UCN depend only on r. In this central force field the equipotential lines are concentric cylindrical shells. Energy E and angular momentum L_ζ about the symmetry axis are conserved. (For vertical systems, L_z is conserved also in the presence of gravity as well as for variable B_ζ, as for end fields, as long as the potential V remains cylindrically symmetric.)

The orbits of the 2D hexapole ($2N = 6$) are ellipses. Analytic expressions for the orbits, in terms of elliptic integrals, exist also for the quadrupole ($2N = 4$), decapole ($2N = 10$) and for $2N = 14$ [33]. Alternatively, the radial equation of motion, $\dot{r} = \sqrt{2[E - V_{\rm eff}(r)]/m}$, in the effective potential $V_{\rm eff}(r) = V(r) + L_\zeta^2/(2m^2r^2)$ is readily solved numerically for any $N(\geqslant 2)$. There are two apsidal radii, $r_{\rm min}$ and $r_{\rm max}$, and the orbits are symmetric about the angular positions of these TPs. Therefore, it suffices to analyze only the path section between any consecutive TPs.

We average over all possible orbits confined within the trap radius R and subject to the requirement of uniform PSD as follows. Choosing the radius $r_1 < R$ of an ES we consider all orbits which turn around at r_1. Subset a of these orbits comes from the inside and has $0 \leqslant r_{\rm min} \leqslant r_1$ and $r_{\rm max} = r_1$. The other subset b of orbits comes from the outside and has $r_{\rm min} = r_1$ and $r_1 \leqslant r_{\rm max} \leqslant R$. In case a (b) the region exterior to the storage space for spin $|+\rangle$ is the range $r > r_1$ ($r < r_1$). In either case, a spin-flipped UCN entering this "forbidden zone" is attracted toward the high field at the wall and considered as lost.

The classification a or b is determined by the peripheral velocity v_1 at r_1: For group a the range of v_1 is between 0 (for the radial path from or toward the center $r = 0$, for which the angular momentum is zero) and $v_c = \sqrt{r_1 F(r_1)/m}$ with centripetal force $F(r_1) = m\,dV/dr_1$. In the latter limit the path is circular with radius r_1. For group b, v_1 ranges from v_c (circular) to v_2 for the limiting path skirting the wall ($r_{\rm max}(v_2) = R$). In each case, the second turning radius and the time $\Delta t(r_1, v_1)$ it takes from one TP to the next are found numerically from the radial equation of motion.

To determine the statistical weight of a given orbit with one TP at radius r_1 we have to modify the strategy used for the UCNτ field. In that case we considered only the sample of orbits where the particle starts from rest at the ES with the highest potential, $V = E/m$, reached for given energy E.

For the cylindrical multipole field (1) only regular orbits exist and releasing a particle from rest would cover only the subset (of measure zero) of trajectories with angular momentum zero, which oscillate radially through O (the axis $r = 0$). However, field (1) is an idealization and in the physical situations field irregularities such as "ripples" and stray fields in the axial ζ direction are unavoidable. As far as the statistics of orbits perturbed in this way goes, the following strategy appears justified: For a path turning around at r_1 with peripheral velocity v_1 we consider the ES of radius ρ such that $V(\rho) = E/m = V(r_1) + v_1^2/2$ and relate the statistical weight for radius ρ to the uniform phase-space density at O. As in Secs. IV A and IV B we differentiate the energy balance between $r = \rho$ and $r = 0$, $E/m = V(\rho) = v_0^2/2$, and obtain the proportionality

$$\frac{\Delta v_0}{\Delta \rho} \sim \frac{dV(\rho)/d\rho}{\sqrt{V(\rho)}}. \tag{14}$$

Multiplying by ρ to take into account the number of allowed points along the circle with radius ρ, we derive the weighting factor for radius ρ, and therefore also the probability $P(r_1, v_1)$ for an orbit with apsidal radius r_1 and apsidal

velocity v_1:

$$P(r_1,v_1) = \rho \frac{dV(\rho)/d\rho}{\sqrt{V(\rho)}} \tag{15}$$

where, by definition of $V(\rho)$ and using (1),

$$\begin{aligned} V(\rho) &= V(r_1) + v_1^2/2 \\ &= (|\mu|/m)\left(\sqrt{B_\zeta^2 + B_{\max}^2(\rho/R)^{2N-2}} - B_\zeta\right). \end{aligned} \tag{16}$$

To evaluate $dV(\rho)/d\rho$ in Eq. (15) we have to take into account the dependence of $V(\rho)$ and of

$$\rho = R\left\{\frac{\left[mV(r_1) + |\mu|B_\zeta + mv_1^2/2\right]^2 - |\mu|^2 B_\zeta^2}{|\mu|^2 B_{\max}^2}\right\}^{1/(2N-2)} \tag{17}$$

[from (16)] on r_1 and v_1:

$$\frac{dV(\rho)}{d\rho} = \frac{\partial V(\rho)/\partial r_1}{\partial\rho/\partial r_1} + \frac{\partial V(\rho)/\partial v_1}{\partial\rho/\partial v_1} = 2\frac{dV(r_1)/dr_1}{\partial\rho/\partial r_1}, \tag{18}$$

where we have used $\partial\rho/\partial v_1 = \{v_1/[dV(r_1)/dr_1]\} \times (\partial\rho/\partial r_1)$ which follows from (17) with the help of $\partial V(\rho)/\partial r_1 = dV(r_1)/dr_1$ and $\partial V(\rho)/\partial v_1 = v_1$. The result is

$$\begin{aligned} &P(r_1,v_1) \\ &= \frac{\mu^2 B_t^2(r_1) + |\mu|B(r_1)mv_1^2 + m^2v_1^4/4}{\left[|\mu|B(r_1) + mv_1^2/2\right]\sqrt{|\mu|[B(r_1) - B_\zeta] + mv_1^2/2}}, \end{aligned} \tag{19}$$

where $B_t(r) = B_{\max}(r/R)^{2N-2}$ and $B(r) = \sqrt{B_\zeta^2 + B_t^2}$ are the multipole fields without and with holding field B_ζ, respectively, and we omitted the constant factor $2(N-1)/\sqrt{m}$.

Weight factor (19) determines how the depolarization rate from (10) is averaged over all paths. At TPs we have $\dot\theta = 0$ since θ depends only on r and $\dot r = 0$. (Here we measure θ from the ζ axis.) The angular velocity of trapping field rotation experienced by a neutron moving through a TP is $\dot\phi = (N-1)v_1/r_1$. Thus, averaging $p/\Delta T$ from (10) over the ensemble of paths, the overall depolarization rate becomes

$$\begin{aligned} \langle 1/\tau_{\rm dep}\rangle = \frac{(N-1)^2}{\nu}\int_{r_1=0}^{R} dr_1 \frac{\sin^2\theta(r_1)}{4r_1^2\omega_L^2(r_1)} \\ \times \int_{v_1=0}^{v_2(r_1)} dv_1\, P(r_1,v_1)\frac{v_1^2}{\Delta t(r_1,v_1)}, \end{aligned} \tag{20}$$

with Larmor frequency $\omega_L(r_1)$ at radius r_1 and normalization constant $\nu = \int_0^R dr_1 \int_0^{v_2(r_1)} dv_1\, P(r_1,v_1)$.

Numerical results for a wide range of multipole orders $2N$ are shown in Fig. 2 for $R = 4.7$ cm and $B_{\max} = 1.3$ T. These are typical values for multipole traps; we keep these parameters the same for hypothetical systems where only the multipole order $2N$ is varied and use $B_\zeta = 0.001$, 0.01, and 0.1 T for the holding field. To show the behavior of $\langle 1/\tau_{\rm dep}\rangle$ vs N more clearly, we have added the half-integral values $N = 5/2$ and $N = 7/2$ which cannot be realized with magnetic fields.

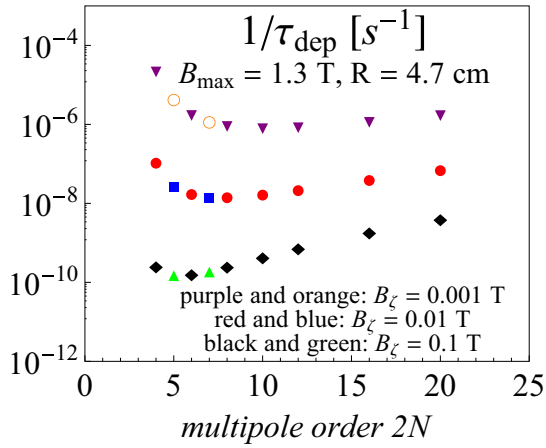

FIG. 2. Mean spin flip rates calculated from Eq. (20) for a cylindrical multipole trap vs order $2N$. The purple, red, and black points (down triangles, closed circles, and diamond symbols) represent integer N; the intervening orange, blue, and green points (open circles, squares, and up triangles) are for half-integral N.

Our calculation for the octupole ($2N = 8$) at $B_\zeta = 1$ mT gives $\langle\tau_{\rm dep}^{-1}\rangle = 1.5 \times 10^{-5}$ s^{-1}. This result is consistent with the order of magnitude $\tau_{\rm dep} = (4 \pm 16) \times 10^4$ s^{-1} given in Table IV of [26] for a solenoid current 3 A, which corresponds to $B_\zeta \gtrsim 1$ mT. (In experiment [26] some depolarization may have been caused by reflection on the Fomblin-coated wall at the bottom of the trap.)

The depolarization rates calculated from (20) for the multipole traps are about 10 times those for the 3D UCNτ field for the same holding field. The difference may be attributed to the small radius $R = 4.7$ cm used. The dimensions of the UCNτ field are larger, $\sim$0.5 m, and therefore the average field gradient is smaller. Our calculation for a cylindrical multipole with large radius $R = 1$ m, a value similar to the multipole design of Ref. [28], gives $\approx 10^2$ times lower spin flip losses for the same values of B_ζ.

We have evaluated expression (20) for the mean depolarization rate, taking into account all possible flight paths subject to the condition of constant PSD and confined to a cylinder of radius R. This was possible since all orbits are regular for model field (1).

By contrast, the orbits in the actual magnetic traps are perturbed and may show instability. In this case we rely on sampling. For instance, for the Los Alamos UCNτ system with its field asymmetry, we have considered, in Sec. IV B, only orbits for which the particle velocity and angular momentum vanish at some time.

Applying the same method to 3D simulations for vertical multipole configurations including gravity would not provide a proper sample of orbits, since these systems conserve angular momentum about the vertical axis, $L_z = 0$. All paths launched from rest would be confined to vertical planes passing through the central axis, as stated earlier.

2. 3D simulations for multipole fields

We include orbits with $L_z \neq 0$ as follows. Choosing a random initial position Q within the trap volume, a particle is

TABLE II. Mean depolarization rate $\langle 1/\tau_{\rm dep}\rangle$ (10^{-9}/s) from 3D simulations for cylindrical multipoles with gravity and end coils included.

$2N$	4	8	20
HOPE, vertical	[4.1(1)]	0.34(1)	[0.78(1)]
HOPE, horizontal	[0.61(1)]	0.15(1)	[0.89(1)]
NIST, mark 2	0.43(1)		
NIST, mark 3	0.021(1)		

launched with initial velocity vector $\mathbf{v}_1$ tangential to the ES at Q and pointing in a random direction within the launch plane. To conform to a uniform distribution in velocity space, the endpoint of $\mathbf{v}_1$ is uniformly distributed within the area of a disk whose radius is determined by the maximum velocity for particle trajectories confined to the trap volume. This and the following operations correspond to those described for the 2D field model (1) in Sec. IV C 1, but averages over the circular ESs of the latter model are now replaced by averages over ESs of general shape in 3D space. Based on (13), this leads to an approximation for the weight factor $P(\mathbf{r}_1,\mathbf{v}_1)$ for launch at position $\mathbf{r}_1$ and initial velocity $\mathbf{v}_1$ and, finally, to the mean depolarization rate $\langle 1/\tau_{\rm dep}\rangle$ by averaging (11) over some 10^3 orbits, each of duration $T_{\rm tot} = 10$ s with $n \gtrsim 500$ TPs.

We approximate the effect of spectral cleaning in UCN storage experiments by specifying the largest energy $E_{\rm max}$ of stored particles. The calculations of $\langle 1/\tau_{\rm dep}\rangle$ shown in Table II use $E_{\rm max} \approx 0.8$ times the value $|\mu|B_{\rm high}$ for the highest field $B_{\rm high}$ in the trap and are based on the field parameters of the following two designs:

(a) The HOPE octupole magnet [26] has bore radius 4.7 cm and its axis is oriented vertically or horizontally. For the vertical configuration we assume activation of only the bottom solenoid with a maximum axial field of 1.4 T while gravity provides the cap. With both end field solenoids activated in the horizontal configuration, we assume fields of 1.4 T on both ends, separated by a distance of 1.13 m, without activating the long holding field solenoid. The radial confinement field is $B_{\rm max} =$ 1.3 T at the trap wall.

(b) Two horizontal Ioffe type quadrupole magnets have been used at NIST [34,35] (versions mark 2 and mark 3). For mark 2 (mark 3) we use maximal fields of axially 1.4 T (4.0 T) and radially 1.3 T (3.9 T), a trap radius of 5 cm (5 cm), and a separation of 0.4 m (0.76 m) between the centers of the end field solenoids; for mark 2, the latter include "bucking" coils [34,35] causing the axial field to drop off more quickly to a minimum of 0.1 T at the trap center. For mark 3, the minimum field is 0.6 T.

Since the depolarization rates depend only weakly on the details of the field distribution, such as field ripples, we use the smoothed fields and approximate the solenoid fields by their values on the solenoid axis, neglecting the variations of field magnitude and direction over the trap's cross section. The results are shown in Table II.

For the HOPE-type system we include, in square brackets, also systems with the same geometries and maximum fields but different multipole order $2N$. We observe the same tendency as for the 2D calculations of Fig. 2: The depolarization rates for $2N = 4$ and $2N = 20$ are higher than in the intermediate range ($2N \sim 8$). This can be explained by higher field gradients, near the axis for low N and near the wall for high N.

As a further general feature, the magnitudes and N dependence of $\langle 1/\tau_{\rm dep}\rangle$ from the 3D simulations in Table II are well approximated by the 2D results from Fig. 2 if we use values of holding field close to their minima: 0.08 T (vertical configuration with $B_{\rm min} = 0.013$ T) and 0.1 T (horizontal with $B_{\rm min} = 0.09$ T) for HOPE [26] and 0.1 T (0.6 T) for NIST mark 2 (mark 3) with $B_{\rm min} \approx 0.1$ T (0.6 T) [34,35].

Finally, $\langle 1/\tau_{\rm dep}\rangle$ approximately scales like B_ζ^{-2}. A similar increase of $\langle 1/\tau_{\rm dep}\rangle$ with decreasing holding field is also seen for UCNτ, as shown by the dashed line in Fig. 1. As an application of scaling in an experiment, we could deliberately lower the holding field to enhance the depolarization loss to a measurable level to verify that the loss for the actual field is negligible.

V. A HIGHER-ORDER SOLUTION

In this section we compare the first-order approximation for the spin-dependent SE, Eqs. (6) and (7), with a higher-order approach where we retain all the terms with A_{pm} and A_{pp} [given in Eq. (5)], which arose from the transformation to the reference system rotating with the field:

$$\dot\alpha + \frac{i\omega_L}{2}\alpha = -A_{pp}\alpha + A_{pm}^*\beta, \tag{21}$$

$$\dot\beta - \frac{i\omega_L}{2}\beta = -A_{pm}\alpha + A_{pp}\beta. \tag{22}$$

The coupled first-order ODEs (21) and (22) can be solved by direct numerical integration with initial conditions $\alpha(0) = 1$, $\beta(0) = 0$ for a particle starting in the $|+\rangle$ state at $t = 0$.

Alternatively, we can use the perturbation approach developed in Ref. [36] for searches for a permanent electric dipole (EDM) of the neutron, to solve the SE for spin 1/2 up to second order of small perturbations. In the EDM case the UCN spin state is perturbed by magnetic field inhomogeneities and a strong static electric field. In Eqs. (21) and (22) the perturbations are the terms on the right-hand side, which are much smaller than those on the left.

To facilitate comparison with [36] we define $\Sigma_{pp}(t) = -2iA_{pp}(t)$ (real-valued), $\Sigma(t) = -2iA_{pm}(t)$ (complex), $\omega_1(t) = \omega_L(t) + \Sigma_{pp}(t)$, and $\Theta_1(t) = \int_0^t \omega_1(t')\,dt'$. In practical cases, Σ_{pp} is at least 10^4 times smaller than ω_L; thus ω_1 is very close to ω_L.

The transformations $\alpha(t) = u(t)\,e^{-i\Theta_1(t)/2}$, $\beta(t) = w(t)\,e^{i\Theta_1(t)/2}$ turn Eqs. (21) and (22) into

$$i\dot u(t) = \frac{1}{2}\Sigma^*(t)\,w(t)\,e^{i\Theta_1(t)},$$

$$i\dot w(t) = \frac{1}{2}\Sigma(t)\,u(t)\,e^{-i\Theta_1(t)}. \tag{23}$$

These coupled ODEs for u and w have the same form as Eqs. (7) for α_r and β_r in Ref. [36]. The only difference is the arguments of the exponential functions. In Ref. [36], the SE

was transformed into the reference frame rotating at constant frequency ω_0 for constant applied Larmor field. In the present case, $\omega_1(t)$ can be an arbitrary function of t; thus the phase factor $e^{\pm i\omega_0 t}$ is replaced by $e^{\pm i\Theta_1(t)}$.

We combine the two first-order ODEs (23) into the single second-order ODE for $u(t)$:

$$\ddot{u}(t) - \left(i\omega_1(t) + \frac{\dot{\Sigma}^*(t)}{\Sigma^*(t)}\right)\dot{u}(t) = -\frac{1}{4}|\Sigma(t)|^2 u(t), \qquad (24)$$

which has the same form as Eq. (8) of [36] with ω_0 in the first term of the expression in brackets replaced by $\omega_1(t)$. This additional time dependence does not affect the method of solving (24) since the second term is time dependent in either case. The initial conditions, $u(0) = 1$ and $w(0) = 0$, are the same as for the EDM case with initial spin up [$\alpha_r(0) = 1$, $\beta_r(0) = 0$].

Following the steps (11) to (18) of [36], we derive

$$w(t) = \frac{2i\dot{u}(t)}{\Sigma^*(t)}\, e^{-i\Theta_1(t)} = -\frac{i}{2}[\Sigma_i(t) - \Sigma_i(0)]$$
$$= -\frac{i}{2}\int_0^t dt'\, e^{-i\Theta_1(t')}\, \Sigma(t'), \qquad (25)$$

where $\Sigma_i(t) = \int dt\, e^{-i\Theta_1(t)}\, \Sigma(t)$.

The initial value, $w(0) = 0$ at $t = 0$, satisfies the required initial condition $\beta(0) = 0$. As t increases, the integral in Eq. (25) rapidly increases on a time scale of order $t_{\min} = 1/\omega_1(0) \approx 1/\omega_L(0)$. In practical applications this is a very short time since the Larmor frequency ω_L is large everywhere inside the trap volume, even at the field minimum where B is the holding field. For $B(0) = 0.01$ T, $t_{\min} = \pi\hbar/(|\mu|B(0)) \approx 3\ \mu$s.

For times $t > t_{\min}$ it is advantageous to change the integration variable in Eq. (25) from t' to Θ_1, with $dt' = d\Theta_1/\omega_1$, and to integrate by parts:

$$w(t) = \left[\frac{\Sigma(t)\, e^{-i\Theta_1(t)}}{2\omega_1(t)}\right]_0^t - \frac{1}{2}\int_0^t dt'\, e^{-i\Theta_1(t')}\frac{d}{dt'}\left[\frac{\Sigma(t')}{\omega_1(t')}\right]. \qquad (26)$$

We did not employ the WKB approximation to derive Eq. (26) but its use enables us to evaluate it analytically: We can neglect the last term in Eq. (26) since the field variable Σ/ω_1 varies slowly on the wavelength scale and get, with (5),

$$\beta(t) = w(t)\, e^{i\Theta_1(t)/2} = \frac{\Sigma(t)\, e^{-i\Theta_1(t)/2}}{2\omega_1(t)}$$
$$= \frac{i}{2\omega_1(t)} e_+(\dot{\theta} + i\dot{\phi}\sin\theta) e^{-i\Theta_1(t)/2}. \qquad (27)$$

In Eq. (27) we have set the integration constant from the lower limit $t = 0$ of the first term in Eq. (26) equal to zero, and an equivalent approximation had also been made in deriving the first-order solution (9) which differs from (27) only by the replacement of ω_1 by ω_L. The detailed justification in Ref. [21], below Eq. (28), can be summarized as follows. Equations (9) and (27) are semiclassical since the SE is solved for the time dependent field $\mathbf{B}(t)$ determined from the classical equations of motion. A fully quantum mechanical treatment requires the solution of the spin and space dependent SE

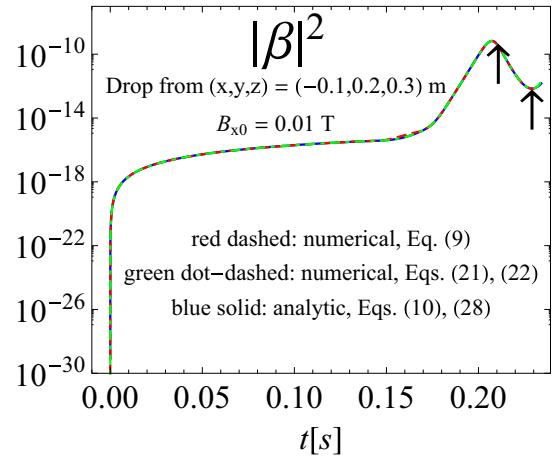

FIG. 3. Magnitude squared of spin flip amplitude β for UCNs released from rest at position $(x,y,z) = (-0.1,0.2,0.3)$ m in the Los Alamos UCNτ "smooth field" [20]. The analytic results, Eqs. (10) and (28) (blue solid), and the numerical solutions of ODE (9) (red dashed) and of ODEs (21) and (22) (green dot-dashed) closely agree. The first two turning points, shown by arrows, are at 0.2108 s (when the particles pass the field minimum at a close distance) and 0.2291 s (when they are reflected at the high field near the wall). The reset of β to zero at these turning points and its subsequent fast increase, within microseconds or less, to the values given by the curves are not shown.

as in Refs. [20,21] and in the Appendix. In this quantum analysis the exact solution for the wave function near a TP involves the Airy functions and the TP is blurred into a nonzero region (typically of order μm). So is the starting time at a TP. Thus, the initial value of the first term in Eq. (26), at $t_0 \approx 0$, which is $\sim e^{-i\Theta_1(t_0)} \approx e^{-i\omega_1(0)t_0}$, should be averaged over the rapidly varying phase $\omega_1(0)t_0$ with the result $\langle e^{-i\Theta_1(t_0)}\rangle_{t_0} = 0$. This holds except for the initial few micrometers of the path subsequent to a TP.

Outside of this region we have, from (27) and (5),

$$|\beta(t)|^2 = |w(t)|^2 = \frac{|\Sigma(t)|^2}{4\omega_1^2(t)} = \frac{|A_{pm}(t)|^2}{\omega_1^2(t)} = \frac{\Omega^2(t)}{4\omega_1^2(t)}. \qquad (28)$$

Equation (28) agrees with the first-order solution (10) if we replace ω_L by ω_1. As we have seen, in practical cases the difference between ω_L and ω_1 is negligible.

Figure 3 shows the time-dependence of spin flip probability $|\beta(t)|^2$ for a particle released from rest at an arbitrary position in UCNτ, here $(x,y,z) = (-0.1,0.2,0.3)$ m, calculated in three ways: (a) The analytic results from Eqs. (10) and (28) (solid curve), and the numerical solutions (b) of differential Eq. (9) (dashed) and (c) of ODEs (21) and (22) (dot-dashed). The three curves closely agree except within short time intervals $t_{\min} \lesssim 10\ \mu$s subsequent to passage through TPs at nonzero velocity, such as the TPs marked by the arrows. The deviations (not shown in Fig. 3) are due to the reset to $\beta = 0$ at a TP. They are shown in detail in Fig. 4 for a UCN moving away from a TP at $(x,y,z) = (-0.1,0.2,0.2)$ m at initial velocity 2 m/s tangential to the local ES. As expected from Eq. (26), $|\beta|^2$ jumps, within a few Larmor periods ($\lesssim 10\ \mu$s), from 0 to the

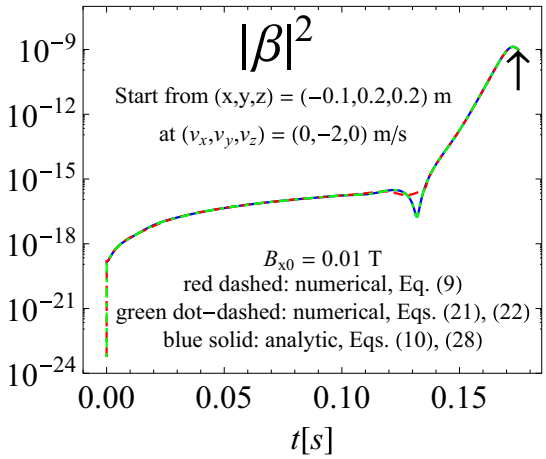

FIG. 4. Spin-flip probability $|\beta|^2$ for UCNs launched in UCNτ at time $t = 0$ from a TP at $(x,y,z) = (-0.1,0.2,0.2)$ m at velocity $(v_x,v_y,v_z) = (0,-2,0)$ m/s (tangential to the local equipotential surface). The numerical integrations of ODE (9) (red dashed) and of ODEs (21) and (22) (green dotted) show the rapid increase, within a few Larmor periods, from $\beta = 0$ at $t = 0$ to the asymptotic behavior given by Eqs. (10) and (28) (blue solid). The ensuing evolution of $|\beta|^2$ up to the next TP (shown by the arrow) is practically unaffected by the transient behavior at $t \approx 0$.

asymptotic curve given by (10) [or (28)]. The remainder of the wave evolution up to the next TP, shown by the arrow, is practically unaffected by the transient at $t \approx 0$.

As a crucial test of the validity of numerical integration of (21) and (22) we verified the norm, $|\alpha(t)|^2 + |\beta(t)|^2$, to be 1 within 1 ppm. The demands on the precision of numerical integration of (9), (21), and (22) become more stringent for paths through regions of higher magnetic field since large Larmor frequencies require short time steps.

VI. SUMMARY AND CONCLUSIONS

The spin flip loss in magnetic storage of UCNs in the Los Alamos UCNτ permanent magnet trap had been analyzed theoretically in Ref. [20] for neutrons on a specific vertical path, and in Ref. [21] for arbitrary motion. In the latter work we used a 1D model for the trapping field. In the present article we have extended this analysis to arbitrary orbits in arbitrary fields in 3D space and report calculations of mean spin flip rates for the UCNτ system and for multipole fields such as the cylindrical octupole of the HOPE project [25,26] and the Ioffe-type quadrupole trapping fields of [23,34,35]. In all cases relevant to magnetic UCN storage we have established agreement between the semiclassical approach, solving the spin-dependent SE for the time-dependent field seen by the particle in a classical orbit, and a fully quantum mechanical analysis based on the space and spin dependent SE solved in WKB approximation. The relative difference between a first-order treatment (in Sec. III) and a higher-order analysis (in Sec. V) of depolarization in the semiclassical framework is at most on the order of 10^{-4} in practical applications.

We confirm and generalize the earlier conclusions of [20,21] relating to "Majorana spin flip at zeros of the magnetic field." Magnetic UCN traps avoid locations of vanishing field by applying a holding field B_h perpendicular to the trapping field. For typical values of B_h we calculate spin flip probabilities which are greater, by many orders of magnitude, than the Majorana prediction [19] which had been derived for fast particles moving in an infinitely extended field rather than the slow UCNs trapped in fields of finite extent. For the magnetic traps investigated we have found an approximate power law behavior of spin flip loss rate as a function of B_h, $\langle 1/\tau_{\rm dep}\rangle \sim B_h^{-2}$ (see Figs. 1 and 2), to be compared with the exponential behavior, $\sim e^{-\pi\xi/2}$ with adiabaticity parameter $\xi = \omega_L/\Omega$, for the Majorana case [19].

Numerical results for the depolarization rate $\langle 1/\tau_{\rm dep}\rangle$ are summarized in Table I and Fig. 1 for UCNτ and in Table II and Fig. 2 for cylindrical multipole fields as for the HOPE and NIST systems. We find good agreement between the analytical calculations for simplified low-dimensional model fields (1D for UCNτ in Ref. [21] and 2D for multipoles in the present Sec. IV C 1) and the more elaborate simulations for 3D field models closer to fields used in experiments. As shown in Fig. 1, $\langle 1/\tau_{\rm dep}\rangle$ strongly depends on B_h and less pronouncedly on multipole order $2N$. For the design fields of HOPE (in horizontal or vertical configuration without activating the long holding field solenoid) we obtained $\langle 1/\tau_{\rm dep}\rangle \sim 10^{-10}$/s. The corresponding values for NIST (mark 3) are $\langle 1/\tau_{\rm dep}\rangle \sim 10^{-11}$/s (see Table II) and $\sim 10^{-9}$/s for UCNτ with $B_h = 0.01$ T (see Table I).

We conclude that B_h can always be increased to a strength that renders spin flip losses negligible compared to other possible sources of systematic error in precision neutron lifetime experiments, foremost that due to marginal trapping. (We leave aside the more fundamental question raised in Ref. [37] whether or not neutron lifetime values derived from storage experiments should indeed be identical to those from beam-type experiments).

ACKNOWLEDGMENTS

We are grateful to P. Huffman for very helpful discussions. K.K.L. acknowledges support under U.S. Department of Energy Contract No. DE-FG02-97ER41042.

APPENDIX: QUANTUM ANALYSIS

The space and spin dependent wave function Ψ for a neutron with energy E moving in a gravito-magnetic trapping field satisfies the SE

$$E\Psi = \left[-\frac{\hbar^2}{2m}\nabla^2 + mgz + |\mu|\boldsymbol{\sigma}\cdot\boldsymbol{B}(x,y,z)\right]\Psi, \qquad \text{(A1)}$$

where $\Psi = \alpha^{(3)}(x,y,z)\chi^+ + \beta^{(3)}(x,y,z)\chi^-$ and σ_x, σ_y and σ_z are Pauli matrices. Superscript (3) indicates that $\alpha^{(3)}(x,y,z)$, for the spin-up wave (relative to the local magnetic field direction), and $\beta^{(3)}(x,y,z)$, for the spin-down wave, are functions of the three spatial coordinates.

The derivatives of χ^+ and χ^- with respect to $j = x,y,z$ are of the same form as the temporal derivatives (4). In terms

of the spin angles θ and ϕ and of $e_\pm = e^{\pm i\phi}$ as defined below Eq. (3) we have

$$\chi_j^+ = \frac{i}{2}\phi_j(1-\cos\theta)\chi^+ - \frac{1}{2}e_+(\theta_j + i\phi_j\sin\theta)\chi^-, \quad \text{(A2)}$$

$$\chi_j^- = \frac{1}{2}e_-(\theta_j - i\phi_j\sin\theta)\chi^+ - \frac{i}{2}\phi_j(1-\cos\theta)\chi^-, \quad \text{(A3)}$$

where the subscript j denotes partial differentiation.

Keeping only the dominant contributions, as in Eqs. (6) and (7), the Laplacian in Eq. (A1) reads

$$\nabla^2\Psi = \left(\alpha_{xx}^{(3)} + \alpha_{yy}^{(3)} + \alpha_{zz}^{(3)}\right)\chi^+ + \left\{\left(\beta_{xx}^{(3)} + \beta_{yy}^{(3)} + \beta_{zz}^{(3)}\right) - e_+\sum_{j=1}^{3}\alpha_j^{(3)}(\theta_j + i\phi_j\sin\theta)\right\}\chi^-. \quad \text{(A4)}$$

Thus, in WKB approximation the spatial wave functions satisfy

$$\nabla^2\alpha^{(3)} + k_+^2\alpha^{(3)} = 0, \quad \text{(A5)}$$

$$\nabla^2\beta^{(3)} + k_-^2\beta^{(3)} = e_+\sum_{j=x,y,x}\alpha_j^{(3)}(\theta_j + i\phi_j\sin\theta), \quad \text{(A6)}$$

where

$$k_\pm^2(x,y,z) = \frac{2m}{\hbar^2}[E - mgz \mp |\mu|B(x,y,z)] \quad \text{(A7)}$$

are the squared local wave numbers for the (+) and (−) spin state, respectively.

Now we consider a UCN with spin (+) starting at time $t = 0$ at a TP and arriving at $t = \Delta T$ at the next TP which we label U. At U the UCN momentarily moves along the local ES at constant speed and we introduce a local Cartesian system of coordinates centered at U with x' and y' in the plane of this ES. z' points away from the direction into which the UCN is reflected.[1] Coordinate system x', y', z' is defined for the narrow space where the ESs can be considered flat (over a region commensurate with the UCN wavelength) and parallel to one another.

Since the $\alpha^{(3)}$ and $\beta^{(3)}$ constituents of the wave function move as a unit the wave numbers $k_{x'}$ and $k_{y'}$ are the same for both. Thus we put

$$\alpha^{(3)}(x',y',z') = \alpha(z')\,e^{ik_{x'}x'}\,e^{ik_{y'}y'},$$
$$\beta^{(3)}(x',y',z') = \beta(z')\,e_+\,e^{ik_{x'}x'}\,e^{ik_{y'}y'}. \quad \text{(A8)}$$

As in Ref. [21], $e_+ = e^{i\phi}$ can be interpreted as a Bloch-wave modulation due to the field rotation.

[1]There are special cases where the path curvature at a TP equals the curvature of the ES. These are locations where two TPs coincide and the trajectory may proceed on either side of the ES, depending on the exact initial conditions. In this limit, the direction "away" is ill-defined, but for a continuous spectral distribution in phase space these paths represent a negligible fraction of the ensemble.

Substituting (A8) in Eqs. (A5) and (A6) we obtain

$$\frac{d^2\alpha(z')}{dz'^2} + k_+'^2(z')\alpha(z') = 0 \quad \text{(A9)}$$

and

$$\left[\frac{d^2\beta(z')}{dz'^2} + k_-'^2\beta(z')\right]e^{ik_{x'}x'}\,e^{ik_{y'}y'} = \sum_{j=x',y',x'}\alpha_j^{(3)}(x',y',z')(\theta_j + i\phi_j\sin\theta), \quad \text{(A10)}$$

where the wave numbers for the z' direction are given by

$$k_\pm'^2 = k_\pm^2 - k_{x'}^2 - k_{y'}^2 \quad \text{(A11)}$$

with $k_\pm^2$ defined in Eq. (A7). Among the components of k_+ and k_-, the z' component $k_+'(z')$ plays a special role. Even within the narrow space where the primed system of coordinates has been defined, k_+' is not constant. It becomes zero at the TP $z' = 0$ and, in this semiclassical picture, is only defined for $z' \leqslant 0$.

In WKB approximation the solution of (A9) is

$$\alpha(z') = \frac{1}{\sqrt{k_+'(z')}}\,e^{iX_+'(z')} \quad \text{(A12)}$$

with $X_+'(z') = \int^{z'} k_+'(u)du$. (The exact quantum solution in form of an Airy function has no singularity at $z' = 0$ and decays exponentially in the classically forbidden zone $z' > 0$.)

To solve (A10) we substitute the WKB approximation for the partial derivatives on the right-hand side, $\alpha_{x'}^{(3)} = ik_{x'}\alpha^{(3)}$, $\alpha_{y'}^{(3)} = ik_{y'}\alpha^{(3)}$, $\alpha_{z'}^{(3)} = ik_+'(z')\alpha^{(3)}$, and implement the total time derivative in the form $d/dt = v_{x'}(\partial/\partial x') + v_{y'}(\partial/\partial y') + v_{z'}(\partial/\partial z')$ with velocity $\mathbf{v} = (\hbar/m)\mathbf{k}_+$. Employing also (A12), (A10) becomes

$$\frac{d^2\beta(z')}{dz'^2} + k_-'^2\beta(z') = \frac{m}{\hbar}\frac{i}{\sqrt{k_+'(z')}}(\dot\theta + i\dot\phi\sin\theta)\,e^{iX_+'(z')}. \quad \text{(A13)}$$

The solution of (A13) has been outlined in Refs. [20,21]. The phase factor for the wave function $\beta(z')$ is the same as for $\alpha(z')$: $e^{iX_+'(z')}$. Therefore, in WKB approximation we have $d^2\beta(z')/dz'^2 = -k_+'^2(z')\beta(z')$ and the solution of (A13) becomes

$$\beta(z') = \frac{m}{\hbar}\frac{i}{\sqrt{k_+'(z')}}\frac{\dot\theta + i\dot\phi\sin\theta}{k_-'^2 - k_+'^2(z')}e^{iX_+'(z')}. \quad \text{(A14)}$$

The depolarization loss measured at TP U is given by the probability current for spin-flipped UCNs,

$$j_-(z') = -\frac{\hbar}{m}\,\mathrm{Re}\left[i\beta^*(z')\left(\frac{d\beta}{dz'}\right)\right], \quad \text{(A15)}$$

leaving the storage space at $z' = 0$ in the positive z' direction. With (A14) this current is

$$j_-(z') = \frac{m}{\hbar}\frac{\dot\theta^2 + \dot\phi^2\sin^2\theta}{[k_-'^2 - k_+'^2(z')]^2} = \frac{\hbar}{m}\frac{\Omega^2}{4\omega_L^2}, \quad \text{(A16)}$$

evaluated at $z' = 0$ (i.e., for the field variables Ω and ω_L at the particle position at time $t = \Delta T$). In the last step of (A16) we have used the Larmor frequency $\omega_L = \hbar(k_-'^2 - k_+'^2)/(2m)$.

To evaluate the spin flip loss rate $1/\tau_{\rm dep}$ between the consecutive TPs we divide the current (A16) by the number $\mathcal{N}$ of (+) spin UCNs moving between the TPs in a channel with unit cross section centered at the trajectory. The cross section of this channel is measured parallel to the ES at every point along the path. The $\mathcal{N}$ particles within this volume contribute to loss current (A16), their decay rate $-\dot{\mathcal{N}}$ equaling $j_-(0)$.

Denoting the wave number perpendicular to the ESs traversed along the way by $k_+'(t)$ and using the WKB form $|\alpha(t)|^2 = 1/k_+'(t)$ as the particle density we have

$$\mathcal{N} = \int_{\rm channel} |\alpha(t)|^2 \, d(\text{volume}) = \int_0^{\Delta T} \frac{1}{k_+'(t)} \frac{\hbar k_+'(t)\, dt}{m} = \frac{\hbar}{m}\Delta T. \tag{A17}$$

As for the 1D field model of [21], $\mathcal{N}$ is given directly by the travel time ΔT. Using (A16), the depolarization rate becomes

$$1/\tau_{\rm dep} = -\dot{\mathcal{N}}/\mathcal{N} = \frac{m}{\hbar}\frac{j_-(0)}{\Delta T} = \frac{\Omega^2}{4\omega_L^2\,\Delta T}, \tag{A18}$$

evaluated for the field at the endpoint U. This agrees with the semiclassical result $1/\tau_{\rm dep} = p(\Delta T)/\Delta T$ with $p(t)$ given by Eq. (10). Generalizing this result to arbitrary time t in the range $t_{\rm min} < t \leqslant \Delta T$ (with $t_{\rm min}$ of order μs), we choose the UCN position at t as the center of reference system x', y', z', with z' normal to the local ES, and use (A14) and (A15) to obtain the identity

$$\frac{m}{\hbar} j_-(t) = \frac{\Omega^2(t)}{4\omega_L^2(t)} = p(t). \tag{A19}$$

This shows that the semiclassical and the quantum approaches to depolarization are equivalent, with $p(t)$ directly corresponding to $m/\hbar$ times the probability current $j_-(t)$.

There is an open question of interpretation: In the derivation of (A13) we used a total time derivative in the form $\dot{f} = v_{x'}(\partial f/\partial x') + v_{y'}(\partial f/\partial y') + v_{x'}(\partial f/\partial z')$ with velocity $\mathbf{v}$ referring to the particle's motion along its classical path. In this sense, the quantum approach of this appendix does involve classical concepts. Use of the WKB method is not the only approximation made.

A similar caveat applies to the possibility of going to higher-order approximations in this quantum approach. In the semiclassical analysis we were allowed to add, in Eqs. (21) and (22), terms such as $A_{pp}\beta$ which are of second order and had been neglected in the first-order Eqs. (6) and (7). However, adding the corresponding second-order contributions in the quantum treatment would require that we also add the second-order quantities neglected in the WKB approximation used to derive the ODEs (A5) and (A6). These would be replaced by coupled nonlinear PDEs of high complexity. At this stage the semiclassical and quantum approaches clearly diverge.

[1] T. Bhattacharya, V. Cirigliano, S. D. Cohen *et al.*, Phys. Rev. D **85**, 054512 (2012).
[2] V. Cirigliano, S. Gardner, and B. R. Holstein, Prog. Part. Nucl. Phys. **71**, 93 (2013).
[3] S. Gardner and B. Plaster, Phys. Rev. C **87**, 065504 (2013).
[4] A. N. Ivanov, M. Pitschmann, and N. I. Troitskaya, Phys. Rev. D **88**, 073002 (2013).
[5] G. Mention, M. Fechner, Th. Lasserre, Th. A. Mueller, D. Lhuillier, M. Cribier, and A. Letourneau, Phys. Rev. D **83**, 073006 (2011).
[6] C. Zhang, X. Qian, and P. Vogel, Phys. Rev. D **87**, 073018 (2013).
[7] A. N. Ivanov, R. Höllwieser, N. I. Troitskaya, M. Wellenzohn, O. M. Zherebtsov, and A. P. Serebrov, Phys. Rev. C **88**, 055501 (2013).
[8] A. Coc, J.-P. Uzan, and E. Vangioni, J. Cosmol. Astropart. Phys. **10**, 050 (2014).
[9] F. Iocco, G. Mangano, G. Miele *et al.*, Phys. Rep. **472**, 1 (2009).
[10] G. J. Mathews, T. Kajino, and T. Shima, Phys. Rev. D **71**, 021302 (2005).
[11] H. Abele, Prog. Part. Nucl. Phys. **60**, 1 (2008).
[12] J. S. Nico, J. Phys. G: Nucl. Part. Phys. **36**, 104001 (2008).
[13] S. Paul, Nucl. Instrum. Methods Phys. Res. A **611**, 157 (2009).
[14] D. Dubbers and M. G. Schmidt, Rev. Mod. Phys. **83**, 1111 (2011).
[15] F. E. Wietfeldt and G. L. Greene, Rev. Mod. Phys. **83**, 1173 (2011).
[16] *Next Generation Experiments to Measure the Neutron Lifetime*, Proceedings of the Workshop, Santa Fe, November 2012, edited by S. J. Seestrom (World Scientific, Singapore, 2014).
[17] V. V. Vladimirskiĭ, Sov. Phys. JETP **12**, 740 (1961).
[18] Yu. N. Pokotilovski, JETP Lett. **76**, 131 (2002); **78**, 422(E) (2003).
[19] E. Majorana, Il Nuovo Cimento **9**, 43 (1932).
[20] P. L. Walstrom, J. D. Bowman, S. I. Penttila *et al.*, Nucl. Instrum. Methods Phys. Res. A **599**, 82 (2009).
[21] A. Steyerl, C. Kaufman, G. Müller, S. S. Malik, and A. M. Desai, Phys. Rev. C **86**, 065501 (2012).
[22] A. Steyerl, C. Kaufman, G. Müller, S. S. Malik, and A. M. Desai, in *2012 Next Generation Experiments to Measure the Neutron Lifetime*, edited by S. J. Seestrom (World Scientific, Singapore, 2014), pp. 75–86.
[23] P. Huffman, C. R. Brome, J. S. Butterworth *et al.*, Nature **403**, 62 (2000).
[24] V. F. Ezhov, A. Z. Andreev, G. Ban *et al.*, Nucl. Instrum. Methods Phys. Res. A **611**, 167 (2009); arXiv:1412.7434.
[25] K. Leung and O. Zimmer, Nucl. Instrum. Methods Phys. Res. A **611**, 181 (2009).
[26] K. K. H. Leung, P. Geltenbort, S. Ivanov, F. Rosenau, and O. Zimmer, Phys. Rev. C **94**, 045502 (2016).
[27] M. Beck, K. Eberhardt, Ch. Geppert *et al.*, in International Workshop: Probing Fundamental Symmetries and Interactions with UCN, April 2016 (unpublished), https://indico.mitp.uni-mainz.de/event/59

[28] S. Materne, R. Picker, I. Altarev *et al.*, Nucl. Instrum. Methods Phys. Res. A **611**, 176 (2009).
[29] W. Paul, F. Anton, L. Paul, S. Paul, and W. Mampe, Z. Phys. C **45**, 25 (1989).
[30] D. J. Salvat, E. R. Adamek, D. Barlow *et al.*, Phys. Rev. C **89**, 052501 (2014).
[31] A. Saunders, M. Makela, Y. Bagdasarova *et al.*, Rev. Sci. Instrum. **84**, 013304 (2013).
[32] P. M. Morse and H. Feshbach, *Methods of Theoretical Physics* (McGraw Hill, New York, 1953), Chap. 9.3.
[33] H. Goldstein, *Classical Mechanics* (Addison-Wesley, London, 1950).
[34] C. R. Brome, J. S. Butterworth, S. N. Dzhosyuk *et al.*, Phys. Rev. C **63**, 055502 (2001).
[35] L. Yang, C. R. Brome, J. S. Butterworth *et al.*, Rev. Sci. Instrum. **79**, 031301 (2008).
[36] A. Steyerl, C. Kaufman, G. Müller, S. S. Malik, A. M. Desai, and R. Golub, Phys. Rev. A **89**, 052129 (2014).
[37] G. L. Greene and P. Geltenbort, Sci. Am. **314**, 36 (2016).